*Journal of New Materials for Electrochemical Systems 15, 63-69 (2012)*


# Ti-doped Lithium Iron Phosphate ($LiFePO_4$) Cathode Materials: Synthesis and Electrochemical Evaluation

Keqiang Ding[1,*], Wenjuan Li[1], Hongwei Yang[1], Suying Wei[2] and Zhanhu Guo[3,†]

[1]College of Chemistry and Materials Science, Hebei Normal University, Shijiazhuang, Hebei 050024, P.R. China
[2]Department of Chemistry and Biochemistry, Lamar University, Beaumont, TX 77710, USA
[3]Integrated Composites Laboratory (ICL), Dan F. Smith Department of Chemical Engineering, Lamar University, Beaumont, TX 77710, USA

Received: November 28, 2011, Accepted: January 09, 2012, Available online: January 25, 2012

***Abstract:*** *The Ti doped $LiFePO_4$ samples, i.e., $LiFe_{1-x}Ti_xPO_4$ (X=0.01, 0.03 and 0.05), were prepared by a modified solid state method. The obtained samples were thoroughly characterized by X-ray diffraction (XRD), scanning electron microscope (SEM) and transmission electron microscope (TEM). XRD patterns indicated that an olivine-type $LiFePO_4$ was fabricated, and SEM images revealed that the particle size of $LiFe_{0.99}Ti_{0.01}PO_4$ was the smallest among the obtained samples. The charge-discharge curves showed that $LiFe_{0.99}Ti_{0.01}PO_4$ delivered the discharge capacity of 153.5 mAh/g at 0.2 C, the largest one among the as-prepared samples, which is rather different from the published report that $LiFe_{0.97}Ti_{0.03}PO_4$ manifested the most promising cycling performance among the samples of $LiFe_{1-x}Ti_xPO_4$ (X=0.01, 0.03, 0.05, 0.07 and 0.09).*

*Keywords: Ti-doping; carbon-coating; $LiFePO_4$; electrochemical performance.*

## 1. INTRODUCTION

Olivine-type $LiFePO_4$ has been widely investigated as a cathode material especially since its first publication by Goodenough and its coworkers in 1997[1]. $LiFePO_4$ has many advantages, including low environmental impact, low cost, and high thermal/chemical stability, when compared to the conventional cathode materials such as $LiCoO_2$, $LiNiO_2$ and $LiMn_2O_4$[2]. However, poor electrical conductivity and weak rate capability have greatly limited its application, especially in the fields of electric vehicles (EV) and hybrid electric vehicles (HEV) [2]. Thus, many methods have been developed to solve the above problems [3]. Generally, there are two typical methods to improve the properties of $LiFePO_4$. The first one is to use carbon-coating or carbon-doping method to enhance the conductivity of the cathode materials. For example, Gu et al.[4] reported the synthesis of $LiFePO_4$-multiwalled carbon nanotubes (MWCNTs) composites prepared by a hydrothermal method, where carbon nanotubes were employed as the carbon sources. Peng et al.[5] published his work on the preparation of $LiFePO_4$/carbon composites fabricated by a soluble starch sol assisted simple rheological phase method. The second is to use metal-element doping, i.e., using a substitutional metal doping for Fe to improve the bulk electronic conductivity. For instance, Jang et al.[6] probed the Cr-doped $LiFePO_4$ and pointed out that the chromium doping can facilitate the phase transformation between triphylite and heterosite during cycling, due to the fact that the doped Cr can replace Fe and/or Li sites in $LiFePO_4$. Wang et al.[7] investigated the Ni-doped $LiFePO_4$ and found that the doped $Ni^{2+}$ not only maintained the phospho-olivine structure of $LiFePO_4$, but also enhanced the electronic conductivity of $LiFePO_4$ greatly, in which the reason to cause these phenomena was not presented. Many metal elements such as Cu [8] and Mn[9] were also doped into $LiFePO_4$, with an intention to enhance the electrochemical performance of $LiFePO_4$.

Ti has been doped into $LiFePO_4$ by many different methods. For example, Wu et al.[10] reported the preparation and characterizations of the $Ti^{4+}$-doped $LiFe_{1-x}Ti_xPO_4$, in which $Ti^{4+}$ was doped in the form of $TiO_2$ and $LiFe_{1-x}Ti_xPO_4$ was synthesized via a solution route followed by a heat-treatment at 700 $^oC$ for 8 hours under $N_2$ flowing condition. The prepared $LiFe_{0.97}Ti_{0.03}PO_4$ powders were

To whom correspondence should be addressed:
Email: *dkeqiang@263.net, †zhanhu.guo@lamar.edu

found to demonstrate the most promising cycling performance. While, Okada et al.[11] reported that Ti doping was not effective to improve the rate capability of $LiMnPO_4$. Wu et al.[12] pointed out that the $TiO_2$-coating imposes a deteriorating effect on the cycle performance of the $LiFePO_4$/carbon composites, though the $TiO_2$ coating reduces the capacity fading of the $LiFePO_4$/Li cells. Thus, the discrepancy on the influence of Ti doping on the electrochemical performance of $LiFePO_4$ intrigued us to probe the Ti doping further.

In the present study, a modified solid-state reaction without inert gas protection was introduced to prepare $LiFePO_4$ doped with different Ti levels in a carbon-coated crucible. $LiFe_{1-x}Ti_xPO_4$ with three different Ti doping levels were synthesized (X=0.01, 0.03 and 0.05). The effects of Ti doping on the particles were investigated. The electrochemical performance of the cells comprised of the obtained samples at room temperature was well measured by cyclic voltammetry (CV) and galvanostatic charge/discharge tests. The possible mechanism of preparing the Ti-doped $LiFePO_4$ was also proposed based on the results from FT-IR spectra and TG-DSC measurement.

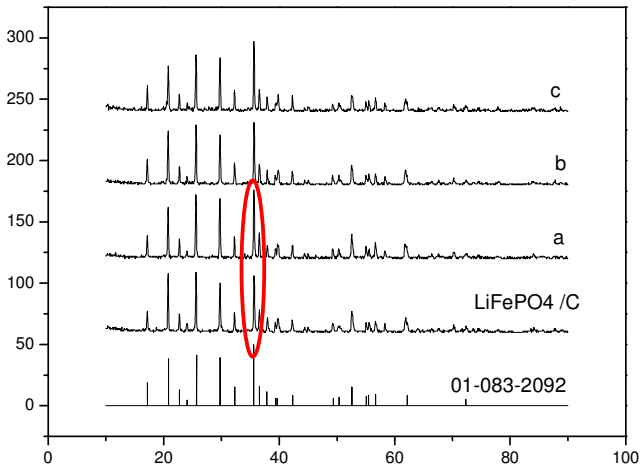


Figure 1. XRD patterns of the as-prepared $LiFePO_4$ samples. (a) $LiFe_{0.99}Ti_{0.01}PO_4$, (b)$LiFe_{0.99}Ti_{0.03}PO_4$ and (c)$LiFe_{0.95}Ti_{0.05}PO_4$. The circled diffraction peaks are used for comparison.

## 2. EXPERIMENTAL

### 2.1. Materials

All the used materials, including $\alpha$-$Fe_2O_3$, $LiOH{\cdot}H_2O$, $NH_4H_2PO_4$, $TiO_2$, glucose and oxalic acid, were all purchased from Tianjin Chemical Reagent Co. Ltd. All materials used in the electrochemical measurement, such as acetylene black, polytetrafluoroethylene (PTFE) binder, electrolyte of 1 M $LiClO_4$ and the cell were all supported by the Tianjin Lianghuo S&T Developing Co. Ltd. All the chemicals are used as-received without any further treatment.

### 2.2. Preparation of $LiFe_{1-x}Ti_xPO_4$

Briefly, based on the molecular formula of $LiFe_{1-x}Ti_xPO_4$ (x = 0.01, 0.03, 0.05), stoichiometric amount of $\alpha$-$Fe_2O_3$, $LiOH{\cdot}H_2O$, $TiO_2$ and $NH_4H_2PO_4$ were mixed thoroughly with 9 wt% glucose and 30 wt% oxalic acid, which was dissolved in distilled water to form a brown-red suspension solution. The solution was then dried at 150 °C for about 13 hours until fluffy powders were obtained. After cooling down to room temperature, the resultant powders were thoroughly ground in a mortar and placed in a crucible. And then the crucible was covered by carbon powder (~10.0 g), leading to a carbon-coated crucible, denoted as a carbon-coating method. The carbon-coated crucible was transferred into an electric furnace with temperature controlled at 700 °C for 3 hours without nitrogen gas flow. As a result, samples of $LiFe_{0.99}Ti_{0.01}PO_4$, $LiFe_{0.97}Ti_{0.03}PO_4$ and Li $Fe_{0.95}Ti_{0.05}PO_4$ were prepared. For comparison, pure $LiFePO_4$ was also prepared by following the above procedures in the absence of $TiO_2$. It should be mentioned that the simplicity and the lower cost are the main advantages of this developed carbon-coating method, when compared to the traditional method using the inert gas as the protection gas.

### 2.3. Characterization

X-ray diffraction (Bruker AXS, D8 ADVANCE, Germany) was used to examine the phase homogeneity. The particle morphology was observed by scanning electron microscopy (HITACHI, SEM S-570) and transmission electron microscopy (HITACHI, TEM H-7650). Fourier transform infrared spectrometry (FT-IR) measurements are carried out on a Hitachi FT-IR-8900 spectrometer (Japan). The thermal behavior of the precursor was characterized with a thermogravimetric anylyzer (TGA7, Perkin-Elmer, USA) and a differential scanning calorimetry (DSC7, Perkin-Elmer, USA) under nitrogen flow. The sample was heated from ambient to 800 $^oC$ at the rate of 10 $^oC$ $min^{-1}$.

The cathodes used for the electrochemical characterization were fabricated by blending the prepared active material powders with acetylene black and polytetrafluoroethylene (PTFE) binder in a weight ratio of 85:10:5. Two-electrode electrochemical cells consisting of lithium metal foil as the negative electrode, Celgard 2400 separator, and an electrolyte of 1 M $LiClO_4$ in ethylene carbonate (EC):diethyl carbonate (DEC):dimethyl carbonate (DMC) (2:5:11, vol.) were assembled in a nitrogen-filled glove box. The electrochemical cycle tests were performed using a LAND series battery testing system (Wuhan Kinguo Electronics Co., Ltd. China) at various rates (1 C=170 mAh/g) between 2.7 and 4.2 V at room temperature.

## 3. RESULTS AND DISCUSSION

### 3.1. Characterization of the as-prepared $LiFe_{1-x}Ti_xPO_4$

Fig. 1 shows the XRD patterns of the prepared samples. The XRD patterns of all the obtained samples are consistent with the

Table 1. Crystal parameters of as-prepared $LiFePO_4$

| samples | Lattice parameters | | | Crystal Cell Volume |
|---|---|---|---|---|
| | a/ Å | b/ Å | c/ Å | V/ (Å$^3$) |
| $LiFePO_4$ /C | 10.319 | 6.001 | 4.693 | 290.61 |
| $LiFe_{0.99}Ti_{0.01}PO_4$/C | 10.322 | 5.997 | 4.702 | 291.06 |
| $LiFe_{0.97}Ti_{0.03}PO_4$/C | 10.321 | 6.003 | 4.693 | 290.76 |
| $LiFe_{0.95}Ti_{0.05}PO_4$/C | 10.317 | 6.005 | 4.692 | 290.68 |

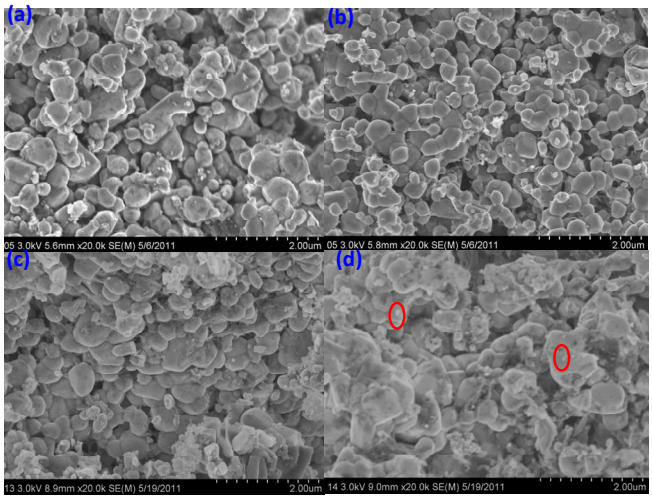


Figure 2. SEM microstructures of the as-prepared **(a)** $LiFePO_4$, **(b)** $LiFe_{0.99}Ti_{0.01}PO_4$, **(c)** $LiFe_{0.97}Ti_{0.03}PO_4$ and **(d)** $LiFe_{0.95}Ti_{0.05}PO_4$. The circled particles in image **d** are thought as $TiO_2$ particles

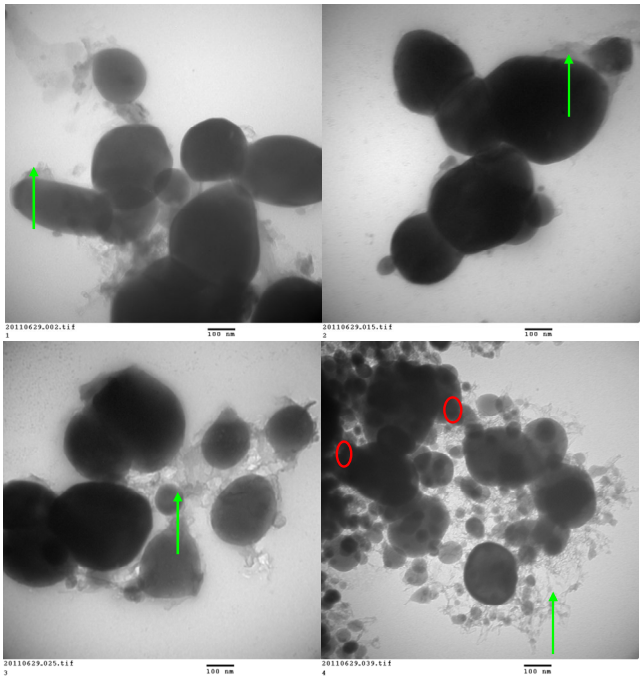

Figure 3. TEM images of the as-prepared samples. Image **(a)** $LiFePO_4$, **(b)** $LiFe_{0.99}Ti_{0.01}PO_4$, **(c)** $LiFe_{0.99}Ti_{0.03}PO_4$and **(d)** $LiFe_{0.95}Ti_{0.05}PO_4$. The marked nano-web structures by green arrows correspond to carbon, and the circled particles in image **d** are $TiO_2$ particles

standard XRD patterns of $LiFePO_4$ very well, indicating that the olivine phase of $LiFePO_4$ is prepared by this carbon-coating method [13]. Based on space group *Pnma*, the lattice parameters obtained from Rietveld refinement are shown Table 1[14]. For pure $LiFePO_4$, the lattice parameters are: a=10.319 Å, b=6.001 Å, c=4.693 Å and V=290.61 $Å^3$, while for $LiFe_{0.99}Ti_{0.01}PO_4$: a=10.322 Å, b=5.997 Å, c=4.702 Å and V=291.06 $Å^3$. These estimated lattice parameters are very close to the reported data of $LiFePO_4$ [15]. For example, the lattice parameters for pure $LiFePO_4$ are reported [16] to be: a=10.2923 Å, b=6.0085 Å, c=4.7126 Å and V=291.4332 $Å^3$. The values of *a*, *c* and *V* for the $LiFe_{0.99}Ti_{0.01}PO_4$ sample are the largest among all the prepared powders, Table 1, indicating the doped one had the widest $Li^+$ ion pathway[17]. Also, the lattice parameter ***b*** of $LiFe_{0.99}Ti_{0.01}PO_4$ is the smallest one among these samples. The decrease of the lattice parameter ***b*** is proposed to shorten the diffusion distance of Li ions and enhance the $Li^+$ intercalation/de-intercalation process[18]. Meanwhile, the intensity of the XRD patterns of the $LiFe_{0.99}Ti_{0.01}PO_4$ powders, the circled part in Figure 1, became slightly stronger when compared to that of pure $LiFePO_4$, which indicates an increased crystallinity [19].

Figure 2 shows the SEM microstructures of the as-prepared samples. Pure $LiFePO_4$ is observed to be irregular and layered particles, Figure 2(a). While for $LiFe_{0.99}Ti_{0.01}PO_4$, more regular and ball-shaped particles are observed, Figure 2(b). With the increase of Ti content, more irregular particles were displayed, Figure 2(c&d). Interestingly, for the $LiFe_{0.95}Ti_{0.05}PO_4$, as shown by the circled particles, some small particles were clearly observed. The morphology of $LiFe_{0.99}Ti_{0.01}PO_4$ is almost identical to that of the reported $LiFePO_4$ [20], in which $LiFePO_4$ was prepared by a one-step microwave method using $CH_3COOLi2H_2O$ and $FeSO_4$ as the starting materials. Obviously, the particle size of $LiFe_{0.99}Ti_{0.01}PO_4$ is the smallest one among the obtained samples. As reported by Gaberscek et al., [21] the smaller size favors the intercalation/de-intercalation process of the Li ions and the discharge capacity drops more or less linearly with increasing the particle size. Thus, $LiFe_{0.99}Ti_{0.01}PO_4$ implies its promising electrochemical performance.

Figure 3 shows the TEM microstructures of the obtained samples. The particle size of the $LiFePO_4$ is in the range from 120 to 310 nm; while the $LiFe_{0.99}Ti_{0.01}PO_4$ particles are in the range from 110 to 350 nm, which is consistent with the SEM observations, Figure 2. For $LiFe_{0.97}Ti_{0.03}PO_4$ and $LiFe_{0.95}Ti_{0.05}PO_4$, the particles sizes are from 100 to 290 nm and from 120 to 240 nm, respectively. Some small particles are also observed in $LiFe_{0.95}Ti_{0.05}PO_4$. Wu et al.[10] pointed out that $TiO_2$ could be observed with TEM in the $Ti^{4+}$-doped $LiFePO_4$ prepared with doping level higher than 5 mol%. Also, the nano-web structures in the light grey region around the particles, marked with arrows in Figure 3, correspond to carbon [22], which favors an enhanced electrical conductivity of $LiFePO_4$[23].

### 3.2. Electrochemical performance of the as-prepared samples

Figure 4 shows the typical charge-discharge curves of the cell at 0.2 C rate using the as-prepared samples as the cathodes. The cells were cycled at 0.2 C rate between 2.7 and 4.2 V vs. $Li/Li^+$, two voltage plateaus at around 3.46 V in the charging cycle and at about 3.38 V in the discharging cycle, corresponding to the lithium deintercalation and intercalation[24], are clearly displayed. And the initial discharge capacity for $LiFePO_4$, $LiFe_{0.99}Ti_{0.01}PO_4$, $LiFe_{0.97}Ti_{0.03}PO_4$ and $LiFe_{0.95}Ti_{0.05}PO_4$ at 0.2 C are 131.6, 153.5, 139.3 and 102.3 mAh/g, respectively. The content of Ti is observed

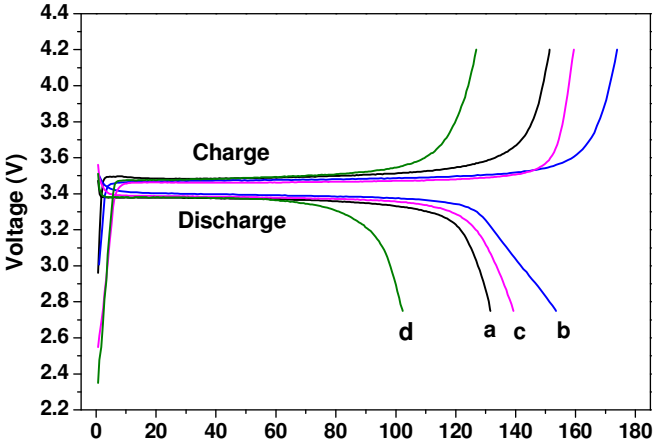


Figure 4. The charge and discharge curves of as-prepared samples of **(a)** $LiFePO_4$;.**(b)** $Fe_{0.99}Ti_{0.01}PO_4$; **(c)** $LiFe_{0.99}Ti_{0.03}PO_4$; and **(d)** $Li\ Fe_{0.95}Ti_{0.05}PO_4$ at 0.2 C.

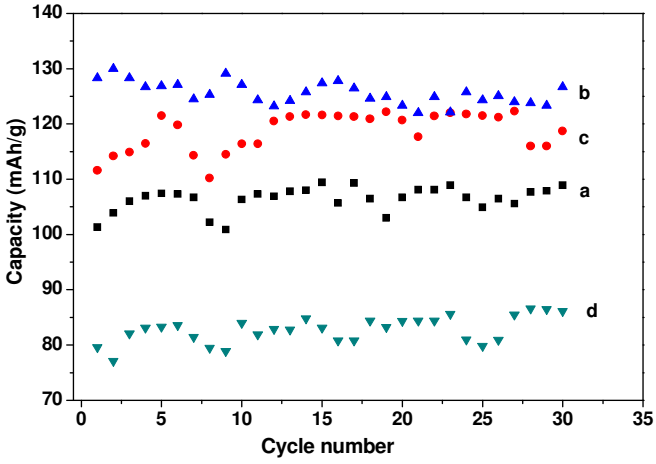


Figure 5. Cycling performance of the cells assembled by obtained samples at 1 C. Lines a, b, c and d are for $LiFePO_4$, $LiFe_{0.99}Ti_{0.01}PO_4$, $LiFe_{0.97}Ti_{0.03}PO_4$ and $LiFe_{0.95}Ti_{0.05}PO_4$, respectively.

to have a dramatic effect on the discharge capacity value. The $LiFe_{0.99}Ti_{0.01}PO_4$ delivered the largest discharge capacity among as-prepared samples. The discharge capacity value of $LiFe_{0.99}Ti_{0.01}PO_4$ is comparative to the value of 157 mAh/g at 0.2 C as reported by Huang et al.[24] While, Wu et al. reported[10] that $LiFe_{0.97}Ti_{0.03}PO_4$ showed the largest initial discharge capacity of 135 mAh/g at 30 °C and 0.1 C rate among the as-prepared samples. The discrepancy is attributed to the different preparation and measuring conditions.

Figure 5 shows the specific discharge capacity of the as-prepared samples as a function of the cycle number at 1 C at room temperature. The discharge capacity for the second cycle corresponding to $LiFePO_4$, $LiFe_{0.99}Ti_{0.01}PO_4$, $LiFe_{0.97}Ti_{0.03}PO_4$ and $LiFe_{0.95}Ti_{0.05}PO_4$ at 1 C is 101.3, 128.3, 111.6 and 79.6 mAh/g, respectively, while after 30 cycles, the discharge capacities are

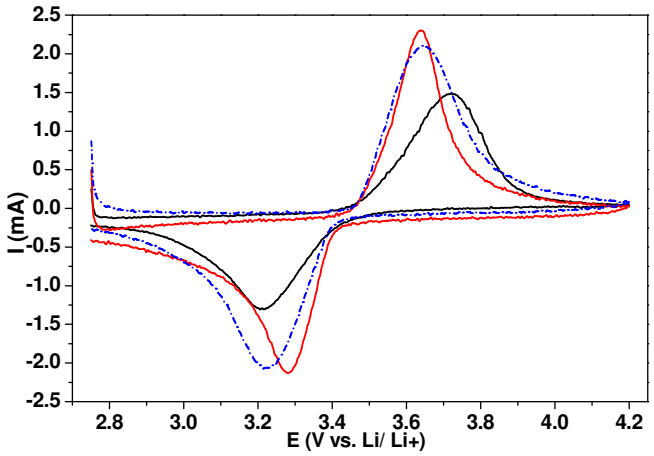


Figure 6. . Cyclic voltammograms (CVs) of the cells assembled by the as-prepared samples. Black, red and blue curves correspond to the cell assembled by pure $LiFePO_4$, $LiFe_{0.99}Ti_{0.01}PO_4$ and $LiFe_{0.97}Ti_{0.03}PO_4$, respectively. Scan rate: 0.5 mV/s.

108.9, 126.7, 118.7 and 86.1 mAh/g, respectively. It can be concluded that a satisfactory cycle performance is well displayed by all samples.

Figure 6 shows the cyclic voltammograms (CVs) of the cells assembled by the as-prepared samples**.** Well-defined redox peaks corresponding to the intercalation/de-intercalation of the lithium ions were observed in all the cells, indicating that Li ions can intercalate/deintercate in/from the as-prepared $LiFePO_4$ freely. For pure $LiFePO_4$, the oxidation and reduction peaks appear at around 3.719 and 3.206 V, respectively. For $LiFe_{0.99}Ti_{0.01}PO_4$ and $Li\ Fe_{0.97}Ti_{0.03}PO_4$, the oxidation and reduction peaks appear at around 3.638 and 3.282 V, 3.640 and 3.215 V, respectively. The peak potential difference $\Delta E_p$ ($\Delta E_p = E_{pa} - E_{pc}$, $E_{pa}$ is the anode peak potential, and $E_{pc}$ is the cathode peak potential) for $LiFePO_4$, $LiFe_{0.99}Ti_{0.01}PO_4$ and $LiFe_{0.97}Ti_{0.03}PO_4$ are 513, 356 and 423 mV, respectively. A smaller peak potential difference $\Delta E_p$ normally indicates a more reversible process [25,26]. Therefore, the reversibility for the intercalation/deintercalation process of the lithium ions in $LiFe_{0.99}Ti_{0.01}PO_4$ is superior to that occurring in $LiFePO_4$ and $LiFe_{0.97}Ti_{0.03}PO_4$. More interestingly, the oxidation peak current and the reduction peak current displayed by $LiFe_{0.99}Ti_{0.01}PO_4$ are both higher than those displayed by $LiFePO_4$ and $Li\ Fe_{0.97}Ti_{0.03}PO_4$. Gu et al.[4] reported that the CVs of Li-$LiFePO_4$, in which $LiFePO_4$ is a composite containing $LiFePO_4$ and multiwalled carbon nanotubes (MWCNTs). At a scan rate of 0.1 mV/s, the oxidation and reduction peaks are reported to appear at around 3.64 and 3.2 V, respectively, and the potential interval between the oxidation and reduction peaks was 440 mV, which is comparable to the potential interval of 356 and 423 mV for $LiFe_{0.99}Ti_{0.01}PO_4$ and $Li\ Fe_{0.97}Ti_{0.03}PO_4$ at the scan rate of 0.5 mV/s.

Electrochemical impedance spectroscopy (EIS) is one of the most powerful tools to analyze the electrochemical reactions, such as those processes occurring at the electrode/electrolyte interfaces and the lithium ion intercalation/deintercalation occurring in anode/cathode[27, 28]. To discuss the role of doping Ti in $LiFePO_4$,

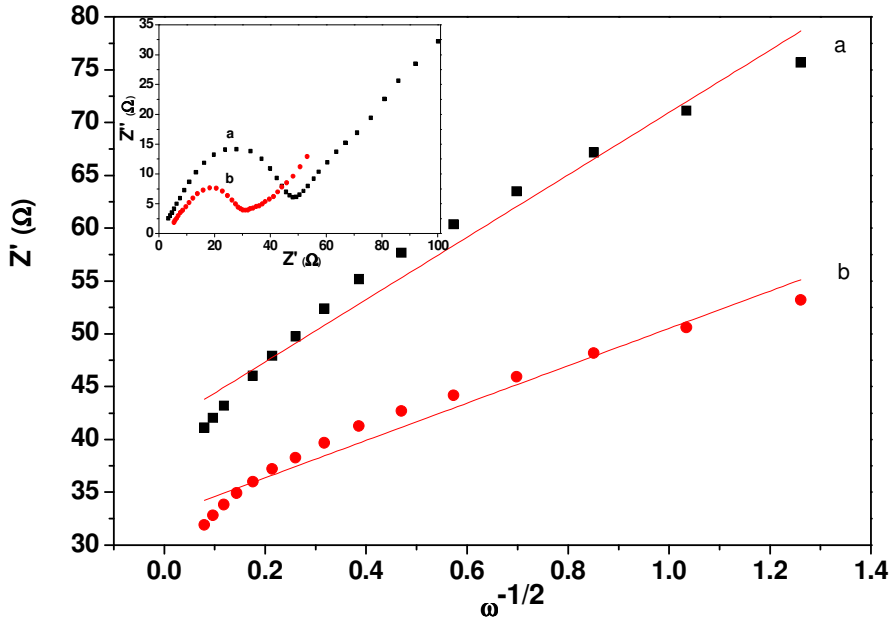


Figure 7. The relationship plot between $Z^{'}$ and $\omega^{-1/2}$ at low-frequency region. The inset is the Nyquist plots obtained for **(a)** $LiFePO_4$ and **(b)** $LiFe_{0.09}Ti_{0.01}PO_4$.

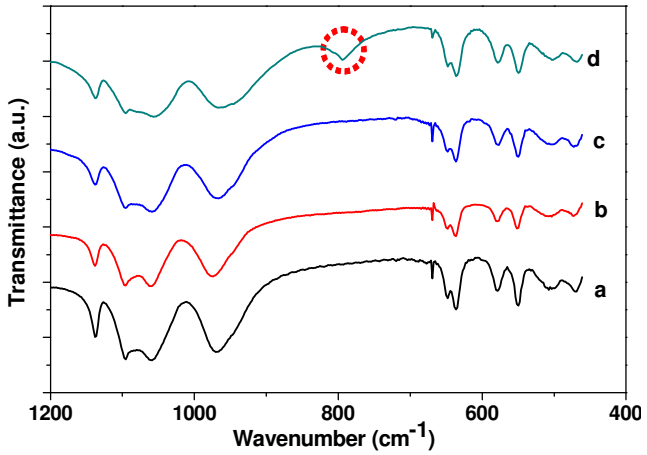


Figure 8. FTIR spectra for as-prepared samples, Curve a, b, c and d correspond to $LiFePO_4$, $LiFe_{0.99}Ti_{0.01}PO_4$, $LiFe_{0.97}Ti_{0.03}PO_4$ and $LiFe_{0.95}Ti_{0.05}PO_4$, respectively. The circled absorption band in line **d** corresponds to the absorption peak of $TiO_2$.

Nyquist plots of $LiFePO_4$ and $LiFe_{0.99}Ti_{0.01}PO_4$ were shown in the inset of Figure 7. Generally, a semicircle in the medium frequency region is related to the charge transfer process and an inclined line in the low frequency region represents the Warburg impedance, which is associated with the lithium-ion diffusion in $LiFePO_4$[4]. The charge transfer resistances ($R_{ct}$) for $LiFePO_4$ and $LiFe_{0.99}Ti_{0.01}PO_4$ from inset of Figure 7 are calculated to be around 51 and 27 Ω, respectively. This indicates that the intercalation/deintercalation process of the lithium ions in $LiFe_{0.99}Ti_{0.01}PO_4$ is easier than that occurring in pure $LiFePO_4$, which is consistent with the results obtained from CVs, Figure 6. Recently Liu et al.[29] reported the $R_{ct}$ of about 300 Ω for pure $LiFePO_4$ and 190 Ω for the $ZrO_2$-coated $LiFePO_4$ composites, which are larger than the value of $R_{ct}$ observed here.

The lithium-ion diffusion coefficient ($D$) can be calculated from Equation (1) [30].

$$D = R^2T^2 / 2A^2n^4F^4c^2\sigma^2 \quad (1)$$

where $R$ is the gas constant, $T$ is the absolute temperature, $A$ is the surface area of the cathode, $n$ is the number of electrons per molecule during oxidization, $F$ is the Faraday constant, $C$ is the concentration of the lithium ions ($7.69\times10^{-3}$ mol/cm$^3$ ) [4], and $\sigma$ is the Warburg factor which is associated with $Z^{'}$. Figure 7 shows the relationship plot between $Z^{'}$ and reciprocal square root of the angular frequency ($\omega$) at low-frequency region. The lithium-ion diffusion coefficients for $LiFePO_4$ and $LiFe_{0.99}Ti_{0.01}PO_4$ are calculated to be $6.87\times10^{-13}$ and $1.92\times10^{-12}$ cm$^2$/s, respectively, which are higher than the reported value of $1.5\times10^{-14}$ cm$^2$/s for the $LiFePO_4$-MWCNTs composites[4], The $D$ value for $LiFe_{0.99}Ti_{0.01}PO_4$ is larger than that of $LiFePO_4$, which is supported by the Nyquist plot, inset of Figure 7. This observation is attributed to the smaller particle size of $LiFe_{0.99}Ti_{0.01}PO_4$ relative to pure $LiFePO_4$ as evidenced by SEM observation, Figure 2, favoring the intercalation/deintercalation process of the Li ions in the cathode materials[21].

To discuss the influence of Ti doping on the obtained samples, FT-IR spectra for all the samples were recorded, Figure 8. The absorption bands centered at 636, 968, 1053, 1094 and 1138 cm$^{-1}$ correspond to the symmetric and asymmetric modes of $PO_4^{3-}$ groups [31]. In the lower wavenumber region, the absorption peaks at 469, 501, 549 and 577 cm$^{-1}$ are attributed to the symmetric and asymmetric bending modes of P–O bonds[30]. In addition, the absence of banks at 762 and 1180 cm$^{-1}$ suggests that the sample is free of $LiFeP_2O_7$[32]. In the sample with the molar ratio of Fe to Ti

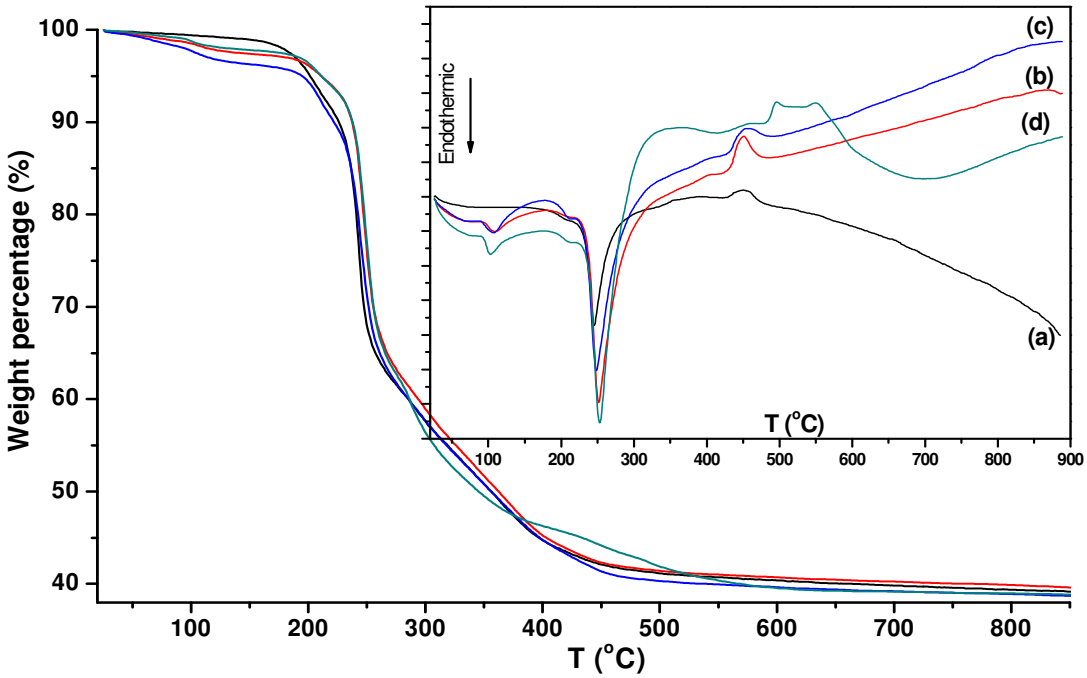


Figure 9. TG-DSC curves of the used precursors for the preparation of sample **(a)** pure $LiFePO_4$, **(b)** $LiFe_{0.99}Ti_{0.01}PO_4$, **(c)** $LiFe_{0.97}Ti_{0.03}PO_4$ and **(d)** $LiFe_{0.95}Ti_{0.05}PO_4$.

95:5, a new absorption peak was observed at around 750 $cm^{-1}$, line **d** of Figure 8, corresponding to $TiO_2$, as observed in the naked rutile $TiO_2$[33].

TG-DSC was used to probe the formation mechanism of the as-prepared samples. TG curves of all the precursors used for the samples comprised three regions, Figure 9. The first region, 150-200 °C, is related to the dehydration of hydrates[34], the second region (230–300 °C) corresponds to the anaerobic thermal decomposition of the starting materials including glucose, oxalic acid and $NH_4H_2PO_4$, and the third region (470–560 °C) is attributed to the complete decomposition of the residual starting materials. No differences are observed in the TG curves of the three precursors, suggesting that the Ti doping does not affect the thermal behaviors of the precursors. While in the DSC curves, obvious differences are observed. The observed endothermic peak at 250 °C, Figure 9, corresponds to the generation of $LiFePO_4$, consistent with the $LiFe_{1-x}Nd_xPO_4$ compounds synthesized with $CH_3COOLi{\cdot}2H_2O$, $FeC_2O_4{\cdot}2H_2O$ and $NH_4H_2PO_4$ as the starting materials [34]. The exothermic peak at around 470 °C in the DSC curve here corresponds to the carbothermal reduction, consistent with the result in the $LiFePO_4$/C composites with $FePO_4{\cdot}4H_2O$ and $LiOH{\cdot}H_2O$ as the starting materials and asphalt powders as carbon source [35]. Interestingly, for the $LiFe_{0.95}Ti_{0.05}PO_4$, the exothermal peak at 470 °C disappeared, instead, two weak new exothermal peaks at around 500 and 580 °C are observed, respectively, suggesting that a new phase transformation took place. To the best of our knowledge, this is the first time to report the TG-DSC curves of the precursors for preparing Ti-doped $LiFePO_4$, though the Ti-doped has been probed by several research groups [10]. TG-DSC curves presented demonstrated that the doped Ti can alter the formation mechanism of $LiFe_{1-x}Ti_xPO_4$ especially when the molar ratio of Fe to Ti is equal to 5%.

## 4. CONCLUSION

The olivine-structure $LiFePO_4$ cathode materials with different Ti doping levels were prepared by a modified solid state reaction method in the absence of inert gas protection. The particle size of the as-prepared samples was observed to be greatly affected by the doped Ti as revealed by SEM and TEM observations. The $LiFe_{0.99}Ti_{0.01}PO_4$ is observed to be the smallest among the obtained samples. The CV and charge-discharge investigations indicates that $LiFe_{0.99}Ti_{0.01}PO_4$ possess the largest initial discharge capacity among the obtained samples, which is rather different from previously published results. FT-IR spectra and TG-DSC reveal the mole ratio of Fe to Ti played an important role in the formation mechanism and the final products.

## 5. ACKNOWLEDGMENTS

This work was financially supported by the National Natural Science Foundation of China (No. 21173066), Natural Science Foundation of Hebei Province of China (No.B2011205014), Key Project Fund of Hebei Normal University (L2008Z08) and Special Assist Project of Hebei Province Personnel Bureau (106115). Z.G. acknowledges the support from the U.S. National Science Foundation (Nanoscale Interdisciplinary Research Team and Materials Processing and Manufacturing) under Grant CMMI 10-30755.

## REFERENCES


[1] A.K. Padhi, K.S. Nanjundaswamy, J.B. Goodenough, J. Electrochem. Soc. 144, 1188 (1997).

[2] D. Jugovic′, D. Uskokovic′, J. Power Sources, 190, 538 (2009).

[3] C. Sun, S. Rajasekhara, J.B. Goodenough, F. Zhou, J. Am. Chem. Soc., 133(7), 2132 (2011).

[4] B. Jin , E. M. Jin , K.-H. Park , H.-B. Gu, Electrochem. Commun., 10, 1537 (2008).

[5] Y. Huang, H. Ren, S. Yin, Y. Wang, Z. Peng, Y. Zhou, J. Power Sources, 195, 610 (2010).

[6] H.C. Shin, S.B. Park, H. Jang, K.Y. Chung, W.I. Cho, C.S. Kim, B.W. Cho, Electrochim. Acta, 53, 7946 (2008).

[7] Y. Ge, X. Yan, J. Liu, X. Zhang, J. Wang, X. He, R. Wang, H. Xie, Electrochim. Acta, 55, 5886 (2010).

[8] J. Morales, J. Santos-Pena, E. Rodríguez-Castellón, S. Franger, Electrochim. Acta, 53, 920 (2007).

[9] T. Nedoseykina, M.G. Kim, S.-A. Park, H.-S. Kim, S.-B. Kim, J. Cho, Y. Lee, Electrochim. Acta, 55, 8876 (2010).

[10] S.-H. Wu, M.-S. Chen, C.-J. Chien, Y.-P. Fu, J. Power Sources, 189, 440 (2009).

[11] T. Shiratsuchi, S. Okada, T. Doi, J. Yamaki, Electrochim. Acta, 54, 3145 (2009).

[12] H.-H. Chang, C.-C. Chang, C.-Y. Su, H.-C. Wu, M.-H. Yang, N.-L. Wu, J. Power Sources, 185, 466 (2008).

[13] B. Wang, Y. Qiu, L. Yang, Electrochem. Commun., 8 ,1801 (2006).

[14] Y. Huang, H. Ren, Z. Peng, Y. Zhou, Electrochim. Acta, 55, 311 (2009).

[15] J. Ni, M. Morishita, Y. Kawabe, M. Watada, N. Takeichi, T. Sakai, J. Power Sources, 195, 2877 (2010).

[16] X. Yin, K. Huang, S. Liu, H. Wang, H. Wang, J. Power Sources, 195, 4308 (2010).

[17] C.Y. Ouyang, D.Y. Wang, S.Q. Shi, Z.X. Wang, H. Li, X.J. Huang, L.Q. Chen, Chin. Phys. Lett., 23, 61 (2006).

[18] L.Q. Sun, R.H. Cui, A.F. Jalbout, M.J. Li, X.M. Pan, R.S. Wang, H.M. Xie, J. Power Sources, 189, 522 (2009).

[19] M.-R. Yang, T.-H. Teng, S.-H. Wu, J. Power Sources, 159, 307 (2006).

[20] Y. Zhang, H. Feng, X. Wu, L. Wang, A. Zhang, T. Xia, H. Dong, M. Liu, Electrochim. Acta, 54, 3206 (2009).

[21] M. Gaberscek, R. Dominko, J. Jamnik, Electrochem. Commun., 9, 2778 (2007).

[22] K.-F. Hsu, S.-Y. Tsay, B.-J. Hwang, J. Mater. Chem., 14, 2690 (2004).

[23] C.H.Mi, X.G. Zhang, X.B. Zhao, H.L. Li, Mater. Sci. Eng., B, Solid-State Mater. Adv. Technol., 129, 8 (2006).

[24] Y. Huang, H. Ren, S. Yin, Y. Wang, Z. Peng, Y. Zhou, J. Power Sources, 195, 610 (2010).

[25] K. Ding, Z. Jia, Q. Wang, X.He, N. Tian, R. Tong, X. Wang, J. Electroanal. Chem. 513, 67 (2001).

[26] K. Ding, Russ, J. Electrochem., 45, 320 (2009).

[27] F. Nobili, S. Dsoke, F. Croce, R. Marassi, Electrochim. Acta, 50, 2307 (2005).

[28] K. Ding, G. Yang, S. Wei, P. Mavinakuli, Z. Guo. Ind. Eng. Chem. Res., 49, 11415 (2010).

[29] H. Liu, G.X. Wang, D. Wexler, J.Z. Wang, H.K. Liu, Electrochem. Commun., 10, 165 (2008).

[30] A.J. Bard, L.R. Faulkner, Electrochemical Methods, second ed., Wiley, 2001, p. 231.

[31] A.A. Salah, P. Jozwiak, J. Garbarczyk, K. Benkhouja, K. Zaghib, F. Gendron, C.M Julien, J. Power Sources, 140, 370 (2005).

[32] K. Zaghib, N. Ravet, M. Gauthier, F. Gendron, A. Mauger, J.B. Goodenough, C.M. Julien, J. Power Sources, 163, 560 (2006).

[33] Y. Zhang, H. Yin, A. Wang, M. Ren, Z. Gu, Y. Liu, Y. Shen, L. Yu, T. Jiang, Appl. Sur. Sci., 257, 1351 (2010).

[34] X. Zhao, X. Tang, L. Zhang, M. Zhao, J. Zhai, Electrochim. Acta, 55, 5899 (2010).

[35] W. Zhang, X. Zhou, X. Tao, H. Huang, Y. Gan, C. Wang, Electrochim. Acta, 55, 2592 (2010).